Icarus 225 (2013) 403–412

Contents lists available at SciVerse ScienceDirect

Icarus

journal homepage: www.elsevier.com/locate/icarus

Wind driven capillary-gravity waves on Titan's lakes: Hard to detect or non-existent?

A.G. Hayes [a,b,*], R.D. Lorenz [c], M.A. Donelan [d], M. Manga [b], J.I. Lunine [a], T. Schneider [e,f,g], M.P. Lamb [g], J.M. Mitchell [h], W.W. Fischer [g], S.D. Graves [g], H.L. Tolman [i], O. Aharonson [g,j], P.J. Encrenaz [k], B. Ventura [l], D. Casarano [m], C. Notarnicola [l]

[a] Center for Radiophysics and Space Research, Cornell University, Ithaca, NY 14853, USA
[b] Department of Earth and Planetary Science, University of California, Berkeley, CA 94720, USA
[c] Applied Physics Laboratory, Johns Hopkins University, Laurel, MD 50742, USA
[d] Rosentiel School of Marine and Atmospheric Science, University of Miami, Miami, FL 33149, USA
[e] Department of Earth Sciences, ETH Zurich, Switzerland
[f] Environmental Science and Engineering, California Institute of Technology, Pasadena, CA 91125, USA
[g] Division of Geological and Planetary Sciences, California Institute of Technology, Pasadena, CA 91125, USA
[h] Department of Earth and Space Sciences, University of California, Los Angeles, CA 90025, USA
[i] Marine Modeling and Analysis Branch, NOAA/NCEP/EMC, College Park, MD 20740, USA
[j] Center for Planetary Science, Weizmann Institute of Science, Rehovot 76100, Israel
[k] Observatoire de Paris, 61 Avenue de l'Observatoire, 75014 Paris, France
[l] Institute for Applied Remote Sensing, EURAC, Bolzano, Italy
[m] CNR-IRPI, Via Amendola 122 I, Bari, Italy

ARTICLE INFO

Article history:
Received 3 March 2012
Revised 12 March 2013
Accepted 10 April 2013
Available online 19 April 2013

Keywords:
Titan
Saturn, Satellites
Radar observations
Infrared observations

ABSTRACT

Saturn's moon Titan has lakes and seas of liquid hydrocarbon and a dense atmosphere, an environment conducive to generating wind waves. Cassini observations thus far, however, show no indication of waves. We apply models for wind wave generation and detection to the Titan environment. Results suggest wind speed thresholds at a reference altitude of 10 m of 0.4–0.7 m/s for liquid compositions varying between pure methane and equilibrium mixtures with the atmosphere (ethane has a threshold of 0.6 m/s), varying primarily with liquid viscosity. This reduced threshold, as compared to Earth, results from Titan's increased atmosphere-to-liquid density ratio, reduced gravity and lower surface tension. General Circulation Models (GCMs) predict wind speeds below derived thresholds near equinox, when available observations of lake surfaces have been acquired. Predicted increases in winds as Titan approaches summer solstice, however, will exceed expected thresholds and may provide constraints on lake composition and/or GCM accuracy through the presence or absence of waves during the Cassini Solstice Mission. A two-scale microwave backscatter model suggests that returns from wave-modified liquid hydrocarbon surfaces may be below the pixel-scale noise floor of Cassini radar images, but can be detectable using real-aperture scatterometry, pixel binning and/or observations obtained in a specular geometry.

1. Introduction

Saturn's moon Titan supports standing bodies of liquid under a dense atmosphere. On Earth, it is rare to observe a body of water whose surface is not disturbed by some form of wave activity (Kinsman, 1984). On Titan, Cassini spacecraft observations through the end of its Equinox Mission in December 2010 show no indication of surface waves in Titan's hydrocarbon lakes and seas (Brown et al., 2008; Wye et al., 2009; Barnes et al., 2011; Hayes et al., 2011; Soderblom et al., 2012). This observation is intriguing given the predominance of aeolian features at equatorial latitudes, which require winds capable of saltating sand sized particles (100–300 μm) (Lorenz et al., 2006). This apparent discrepancy may result from differences between expected wind speeds and the conditions required for wave generation on Titan and Earth.

The physical and environmental parameters associated with exciting wind-driven waves on Titan were recently reviewed by Lorenz et al. (2010b). Lorenz and Hayes (2012) discuss the growth of pre-existing waves in the gravity regime, accounting for Titan's environmental conditions. Wind-generated waves on Titan were initially studied by Ghafoor et al. (2000), who scaled terrestrial expressions of wave height to Titan gravity but ignored the effects of viscosity, density, and surface tension. Wind tunnel experiments by Lorenz et al. (2005), who used kerosene as a Titan sea analog, and Donelan and Plant (2009), who varied the temperature of water,

---

* Corresponding author.
E-mail address: hayes@astro.cornell.edu (A.G. Hayes).

0019-1035/$ - see front matter © 2013 Elsevier Inc. All rights reserved.
http://dx.doi.org/10.1016/j.icarus.2013.04.004

show that some or all of these factors can substantially affect the threshold for wave generation. This work differs from previous studies by simultaneously accounting for the gravity, viscosity, surface tension, and air/liquid density relevant to the Titan environment.

Here, we investigate analytically the conditions necessary for the onset of exponential growth in capillary-gravity wave amplitude in Titan's lakes using modern theories of wind wave generation. In addition, we adapt the two-scale microwave backscatter model of Donelan and Pierson (1987) to the Titan environment and investigate the expected Ku-band response of modeled wave spectra based on predicted wind speeds from the General Circulation Model (GCM) of Schneider et al. (2012). For liquid compositions varying between pure methane and equilibrium mixtures with the atmosphere, we find that the threshold wind speed for wave generation is 2.5–4.5 times lower than on sea-water on Earth at 30 °C, depending primarily on liquid viscosity. While polar equinoxial winds are predicted to have been calm, consistent with the observed absence of wave activity, winds speeds are predicted to increase during northern spring and summer. This more lively wind regime, which will be investigated during the Cassini Solstice Mission, is predicted to produce wind speeds capable of exceeding the modeled thresholds and potentially exciting wind waves. The time and frequency of wave activity (or lack thereof) observed during the Solstice Mission may provide constraints on liquid composition through the viscosity dependence of threshold wind speeds.

2. Generating capillary-gravity waves

Wind blowing over a liquid surface generates waves that grow in amplitude with increasing wind speed. Energy can be transferred from the wind to the waves by either pressure fluctuations or tangential stresses (Kinsman, 1984). Phillips (1957) developed a theory for wave generation, known as the resonance mechanism, where waves are initiated and grow in resonance with turbulent air pressure fluctuations. Turbulent eddies are advected over the liquid surface at some velocity related to the wind. Resonance is only possible if the waves are traveling along with the turbulence, leading to a minimum wind speed necessary for excitation that is correlated to the minimum phase speed of the waves (see below). Since the turbulent pressure fluctuations are in random phase with respect to the surface waves, the resonance mechanism can only account for linear growth (similar to a random walk). Resonance waves are small (10's of micrometers amplitude) and are not responsible for the observable disturbances typically associated with wind waves (Kahma and Donelan, 1988). The resonance mechanism is thought to be responsible for the excitation and initial growth of waves on an undisturbed liquid surface and for the rhomboidal structure of newly emerging wave fields (Kinsman, 1984).

Surface waves exhibit a minimum phase speed (c) because of the competing effects of gravity (g) and surface tension (γ), which are related through the dispersion relation for deep water waves ($\coth(kd) \approx 1$). The potential energy in a gravity wave is proportional to the square of its wavelength, and so in the absence of other effects, higher wavenumbers would be favored. However, the potential energy of a capillary wave restored by surface tension is proportional to the curvature of the wave, and so is greatest at large wavenumbers. There naturally exists a wavenumber (and associated phase speed) that minimizes the total potential energy of a surface wave given these two restoring forces. Wind-driven gravity waves are not observed below this minimum, presumably because the surface must first be corrugated for the wind to exert a force against it, and corrugation of a flat surface is produced when surface stress overcomes surface tension. Gravity waves then emerge and grow having been seeded by capillary waves. The phase speed of surface waves, given by the dispersion relation, is (Kinsman, 1984):

$$c^2 \approx \gamma k/\rho_f + g/k, \tag{2.1}$$

where k is the wavenumber, γ is the surface tension, ρ_f is the liquid density, d is the liquid layer depth, and g is gravity. Table 1 lists the values of these and other parameters relevant to wind wave generation on Earth and Titan. Fig. 1 shows the phase speed for terrestrial seawater and ethane/methane liquids on Titan. At large wavelengths, gravity is the dominant restoring force and wave energy increases with increasing wavelength. For smaller wavelengths, surface tension is the dominant restoring force and wave energy increases with decreasing wavelength (increasing curvature). Waves dominated by gravity are known as gravity waves while waves dominated by surface tension are known as capillary waves. Waves for which both restoring forces are important are known as capillary-gravity waves. For seawater, surface tension can be neglected (to within 95% confidence in determining the phase speed) for $\lambda > 5$ cm while gravity can be neglected for $\lambda < 0.5$ cm. For liquid hydrocarbon on Titan, gravity waves can be defined as $\lambda > 10$ cm and capillary waves exist for $\lambda < 1$ cm.

The phase speed has a minimum value $c_{\min} = (4\gamma g/\rho_f)^{1/4}$ that occurs at $k_{\min} = \sqrt{g\rho_f/\gamma}$. On Earth, these waves are the easiest to be initially excited by wind, have a wavelength of 1.7 cm and travel at a speed of 0.23 m/s. On Titan, the slowest moving waves are expected to have a wavelength ($\lambda = 2\pi/k$) of 3 cm and move at 0.11 m/s (using the parameters listed in Table 1). In general, phase speeds for water on Earth are approximately twice as fast as phase speeds for liquid hydrocarbon on Titan for wavelengths in Titan's capillary-gravity regime (1 cm < λ < 10 cm).

Once initial wavelets are generated their presence can modify the air flow in the boundary layer above them, generating additional pressure fluctuations. These wave-induced pressure fluctuations are in-phase with the topographic wave slope and can lead to exponential growth. Miles (1957) rigorously studied the possibility of energy transfer between the mean air flow and a wavy liquid surface, obtaining estimates for the wind speed necessary to trigger the onset of exponential growth that were in general agreement with field observations. Prior to the work of Miles, Jeffreys (1924) had postulated that energy transfer to waves occurs through form drag. Jeffreys (1924) did not, however, provide a theoretical method for deriving the proportionality constant in his theory, known as the sheltering coefficient. Together, the independent and complimentary work of Phillips (1957) and Miles (1957) is collectively known as the Miles–Phillips theory, which is generally agreed to be the cornerstone on which modern wind wave generation models are built (Young, 1999). Recently, the threshold associated with the onset of exponential growth has been observed experimentally by Donelan and Plant (2009), providing support for the concept of a positive feedback mechanism between growing surface waves and airflow in the boundary layer. While a detailed derivation of the Miles–Phillips theory is outside the scope of this work, Fig. 2 depicts the physical picture by which the resonance (Phillips, 1957) and instability (Miles, 1957) mechanisms generate pressure gradients to excite wind-waves.

In addition to the Miles–Phillips theory, Kelvin–Helmholtz (KH) instabilities are also known to excite waves at the interface between two fluids. The classical KH theory considers a tangential discontinuity between uniform flows of air over water (Thomson, 1871). Miles (1959) updated the theory to account for logarithmic velocity profiles in the upper fluid (air). For "air over water" the KH mechanism, which is independent of fluid viscosity, predicts threshold wind speeds that are an order of magnitude larger than observed. The KH mechanism correctly predicts wind thresholds, however, for highly viscous and/or contaminated liquids, where small-scale waves are damped by viscous dissipation (Miles, 1959). Shtemler et al. (2008) argues that the KH mechanism may

Table 1
Physical parameters associated with wind wave generation on Earth and Titan. Kinematic viscosities (ν_f) represent seawater between 0 °C and 30 °C on Earth and hydrocarbon mixtures ranging from pure CH_4 to the more complex compositions predicted by Cordier et al. (2009) at 94 K on Titan. Complex dielectric constants for seawater and liquid hydrocarbon are from Saxton and Lane (1952) and Paillou et al. (2008), respectively. The kinematic viscosity of Titan's atmosphere (ν_a) is taken to be that of nitrogen gas at 94 K. The remaining parameters are referenced from Weast (1984) for Earth and Lorenz et al. (2010b) for Titan. The observing wavenumber (k_o) and wavelength (λ_o) corresponds to the RADAR instrument onboard the Cassini spacecraft and $\lambda_{\min}$ is the wavelength of a surface wave moving at the minimum phase speed ($c_{\min}$). The minimum phase speed is defined as $c_{\min} = (4\gamma g/\rho_f)^{1/4}$ (Section 2.1).

Parameter	Description	Earth	Titan
ϵ	Liquid dielectric constant	53.98 + 34.38*i*	1.75 + 0.002*i*
ρ_a	Air density	0.0012 g/cm^3	0.005 g/cm^3
ρ_f	Liquid density	1.03 g/cm^3	0.531–0.662 g/cm^3
ν_a	Air viscosity	0.154 cm^2/s	0.0126 cm^2/s
ν_f	Liquid viscosity	0.0084–.0184 cm^2/s	0.003–0.03 cm^2/s
g	Gravity	981 cm/s^2	135 cm/s^2
γ	Liquid surface tension	73 dynes/cm	18 dynes/cm
$c_{\min}$	Minimum phase speed	23.0 cm/s	11.0–11.6 cm/s
$\lambda_{\min}$	Wavelength at $c_{\min}$	1.7 cm	2.8–3.2 cm
λ_o	Cassini RADAR wavelength		2.16 cm
k_o	Cassini RADAR wavenumber		2.9 cm^{-1}

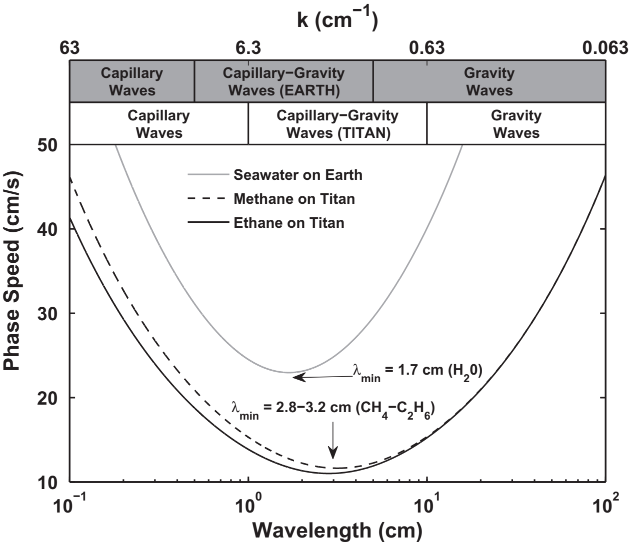

Fig. 1. Phase speed (c) for waves traveling in seawater on Earth and liquid hydrocarbon on Titan calculated from the dispersion relation (Eq. (2.1)) using the physical parameters listed in Table 1.

be important for longer wavelength waves at high wind speeds. The modified KH theory of Miles (1959) predicts threshold wind speeds of at least 3 m/s for liquid hydrocarbon on Titan, which is greater than even the strongest expected winds (see Section 5). Predicted liquid viscosities on Titan (see Table 1), however, are within the range of applicability for the Miles–Phillips theory (i.e., viscous dissipation does not overwhelm energy transfer through shear-flow instability); as such, the remainder of this section will focus on applying the exponential growth (feedback) theories and their more modern variants to the Titan environment.

2.1. Applying wind wave generation models to Titan

Resonance can occur when turbulent eddies of the appropriate length-scale are advected at the phase speed of a growing wave. Under the assumption of frozen turbulence, Elliot (1972) found that the convection velocity appropriate for exciting resonance waves of wavenumber k is the wind speed at an elevation of $\sim\pi/k(=\lambda/2)$. For an aerodynamically smooth surface and logarithmic wind velocity profile (Eq. (2.3)), a wind speed equal to the minimum phase speed $c_{\min} = 0.11$ m/s at a height of $z = \pi/k_{\min} = 1.5$ cm corresponds to a wind speed at 10 m of $U_{10} = 0.22$ m/s. This suggests that the minimum wind speed necessary to excite resonance waves on Titan is $U_{10} = 0.22$ m/s. The wind speed at 10 m (U_{10}) is a universally standard meteorological measurement height (National Renewable Energy Laboratory, 1997) and is adopted here to facilitate comparison with the terrestrial oceanographic literature. On Earth, resonance waves have significant wave heights of ~10 μm (see Section 3) and RMS slopes of a few tens of microradians, making them very difficult to observe; they are typically identified through the presence of glimmers on an otherwise smooth surface (Kahma and Donelan, 1988). While these disturbances may be a factor of a few larger on Titan, they will still be well below the detection threshold of current instrumentation. Regardless, resonance waves may provide the initial disturbances required for the onset of exponential growth and subsequent generation of readily observable waves.

Once initial wavelets are generated, Miles (1957) derived a model for the exponential growth rate of capillary-gravity waves (β_g) based on a positive feedback between the waves and the wind in the boundary layer, assuming a logarithmic velocity profile:

$$(\beta_g/\omega)_{Miles} = \zeta_M \frac{\rho_a}{\rho_f}(u_\star/c)^2 \cos^2(\chi - \bar{\chi}), \tag{2.2}$$

where $\omega = ck$ is the angular frequency of the growing wave, $(\chi - \bar{\chi})$ is the deviation between the directions of wind and wave propagation, $u_\star$ is the friction velocity, ρ_a is the air density, and ζ_M is a dimensionless coefficient known as the Miles parameter. The Miles parameter is proportional to the ratio between the curvature and slope of the wind profile at the critical height where the wind speed equals the phase speed of the growing wave (Miles, 1957). The friction velocity, by definition, is proportional to the square root of the applied surface stress ($\tau = \rho_a u_\star^2$) and can be related to the wind-velocity profile near the air–liquid interface as:

$$U(z) = \frac{u_\star}{\kappa} \ln\frac{z}{z_o}, \tag{2.3}$$

where κ is the Von-Kármán turbulence constant ($\kappa = 0.41$, Garratt, 1977), z_o is the total roughness length, and z is the height above the surface. Following Smith (1988), the total roughness length during the initial stages of wave generation is approximated by the combination of the aerodynamic roughness length of the short surface waves ($z_c = \alpha_c u_\star^2/g$) (Charnock, 1955) and the roughness length for an aerodynamically smooth surface ($z_s = 0.11\nu_a/u_\star$, where ν_a is the kinematic viscosity of the air) (Businger, 1973):

$$z_o = z_c + z_s = \alpha_c u_\star^2/g + 0.11\nu_a/u_\star. \tag{2.4}$$

where α_c is the Charnock parameter, which depends on wave age $\frac{c}{U_{10}}$, and 0.11 is an experimental value related to the Von-Kármán

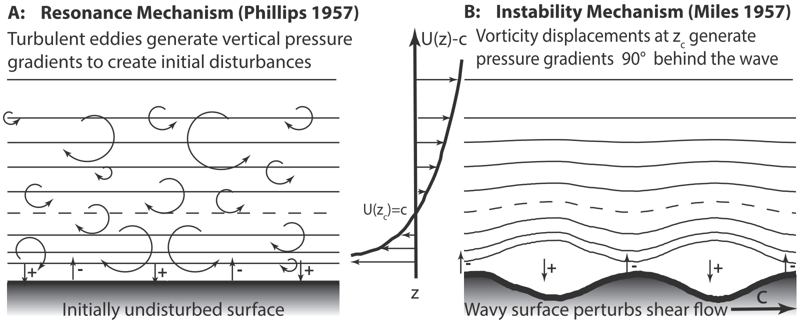

Fig. 2. Physical depiction of how the resonance (e.g., Phillips, 1957) and instability (e.g., Miles, 1957) mechanisms generate vertical pressure gradients to excite wind waves. For a detailed review of these mechanisms see, e.g., Kinsman (1984) or Young (1999). (A) Resonance Mechanism: Turbulent eddies are advected over the liquid surface. If the horizontal scale of the associated vertical pressure gradients are similar to the wavelength of surface waves with phase speeds equal to the advection rate, the waves will linearly grow. (B) Instability Mechanism: In the critical layer ($U(z_c) = c$), local concentrations of excess vorticity peak over the nodes (positions of maximal slope) of the surface waves that are perturbing the shear flow. This vorticity field induces a velocity field which redistributes the vorticity field, which . . .. Feedback between these induces fields at the critical layer lead to a pressure component with a $\pi/2$ phase lag relative to the surface waves. These pressure gradients are therefore in phase with the topographic wave slope and lead to exponential growth. Panel B is adapted from Lighthill (1962).

constant (Nikuradse, 1933), which is assumed to be a universally independent (e.g., Barenblatt and Chorin, 1998). Garratt (1977) found $\alpha_c = 0.0144$ for a variety of sea states. To derive a threshold for the onset of capillary-gravity waves, Miles (1957) balanced the growth rate (Eq. (2.2)) against the loss rate associated with viscous dissipation:

$$\beta_{\nu_f}/\omega = 4\nu_l k/c. \tag{2.5}$$

Two modern variants of the exponential growth theory, which are commonly used to predict the onset of observable wind waves in the capillary-gravity regime, are Plant (1982) and Donelan and Pierson (1987). For sea water both predict minimum threshold wind speeds at $z = 10$ m $\left(U_{10}^{th}\right)$, i.e., the wind speed at which wave growth balances loss by viscous dissipation, between 1.5 m/s and 2 m/s depending on sea temperature (i.e., viscosity). Similar to Miles (1957), Plant (1982) relates the exponential growth of capillary-gravity waves to the square of the friction velocity using Eq. (2.2), but assumes a constant Miles parameter ($\zeta_{M_{Plant}} \sim 34.3$). Donelan and Pierson (1987), on the other hand, more closely follow the sheltering theory of Jeffreys (1924) and boundary layer dynamics of Elliot (1972), and relates the growth rate to the wind speed at a height $z = \lambda/2$ above the mean water level ($U_{\lambda/2}$):

$$(\beta_g/\omega)_{Donelan} = 0.194\frac{\rho_a}{\rho_f}[(U_{\lambda/2}/c)\cos(\chi - \bar{\chi}) - 1]^2 \tag{2.6}$$

where β_g is only defined for $(U_{\lambda/2}/c)\cos(\chi - \bar{\chi}) > 1$ and zero otherwise. Donelan and Pierson (1987) prefer a reference height of $\lambda/2$ as opposed to the critical height of Miles (1957) because it both scales with the size of the roughness elements affecting the boundary layer (i.e., waves) and is sufficiently high to clear their amplitudes. For even moderate winds, the critical height of Miles (1957) can descend below the wave-crests and, for high $u_\star$, asymptotically approaches z_o. For a wave to grow, the wind speed at $\lambda/2$ must exceed the phase speed, $(U_{\lambda/2}/c)\cos(\chi - \bar{\chi}) > 1$, and the growth rate must be greater than loss from viscous dissipation ($\beta_g > \beta_{\nu_f}$). The dimensionless constant 0.194 has been experimentally found to be valid over a range of liquid temperatures (i.e., variations in ρ_f and ν_f) (Donelan and Plant, 2009) and, more recently, under Martian atmospheric conditions (Banfield et al., 2012).

Donelan and Plant (2009) performed experimental work in a wave tank to compare the models of Plant (1982) with Donelan and Pierson (1987) and found that $U_{\lambda/2}$ was a more reliable estimate for the onset of capillary-gravity waves and that initial growth did not occur in a constant-stress environment, as was predicted by the theory of Plant (1982). At larger wind speeds, the two theories were indistinguishable. They also observe that the threshold wind speeds were independent of fetch (downwind length of liquid surface).

Following the results of Donelan and Plant (2009), we will use the theory of Donelan and Pierson (1987) to estimate the wind wave threshold for liquid hydrocarbon on Titan. While Eq. (2.6) has not been experimentally validated under Titan conditions, its derivation allows for variations in the relevant physical parameters (ρ_a, ρ_f, g, and γ). The threshold is derived by equating growth (Eq. (2.6)) with viscous dissipation (Eq. (2.5)) and solving for $U_{\lambda/2}$. For a given $U_{\lambda/2}$, $u_\star$ and z_o can be estimated using Eqs. (2.3) and (2.4). U_{10} can then be calculated using Eq. (2.3). Fig. 3 shows threshold wind speed $\left(U_{10}^{th}\right)$ for waves in the capillary-gravity regime using both the Miles (1957) and Donelan and Pierson (1987) formulations. In both cases, the dependence on z_o is weak because it enters only logarithmical and thus does not significantly effect U_{10}^{th}. For viscosities ranging between pure methane ($\nu_f = 0.0031$ cm^2/s) and the more complex equilibrium compositions predicted by Cordier et al. (2009) ($\nu_f = 0.026$ cm^2/s), U_{10}^{th} ranges between 0.4 and 0.7 m/s. For pure ethane at 94 K ($\nu_f = 0.017$ cm^2/s), $U_{10}^{th} \sim 0.6$ m/s.

Without accounting for surface tension, viscosity, or gravity, Lorenz et al. (2010b) suggested a threshold wind speed of 0.5–1.0 m/s for wave generation on Titan based on scaling Earth observations assuming a square-root relationship with atmospheric density. This is surprisingly similar to our result of 0.4–0.7 m/s, which includes dependencies for surface tension, viscosity, gravity, and atmospheric/liquid density. Lorenz et al. (2010b) do not assign an altitude to the reported threshold speed and the reported range is based on the variation in published wave generation thresholds documented on lake and ocean surfaces. The threshold wind speeds reported herein are reported for an elevation of 10 m and the variation is correlated to the range of liquid viscosities expected in the Titan environment.

3. The complete wave spectrum

In order to study the size and detectability of emerging wave fields on Titan, we need to understand the amplitude spectrum expected for a given wind speed. At high wavenumbers (short wavelengths), the equilibrium wave function is a balance between energy input from the wind and the dissipative processes associated with liquid viscosity, wave breaking, and non-linear parasitic interactions (Donelan and Pierson, 1987):

$$\Phi(k,\chi)_{short} = k^{-4}[(\beta_g/\omega - \beta_\nu/\omega)/\alpha]^{1/n}, \tag{3.1}$$

where n and α are semi-empirical functions of $k/k_{\min}$, defined in Donelan and Pierson (1987), that approximate dissipation due to wave breaking and parasitic ripples:

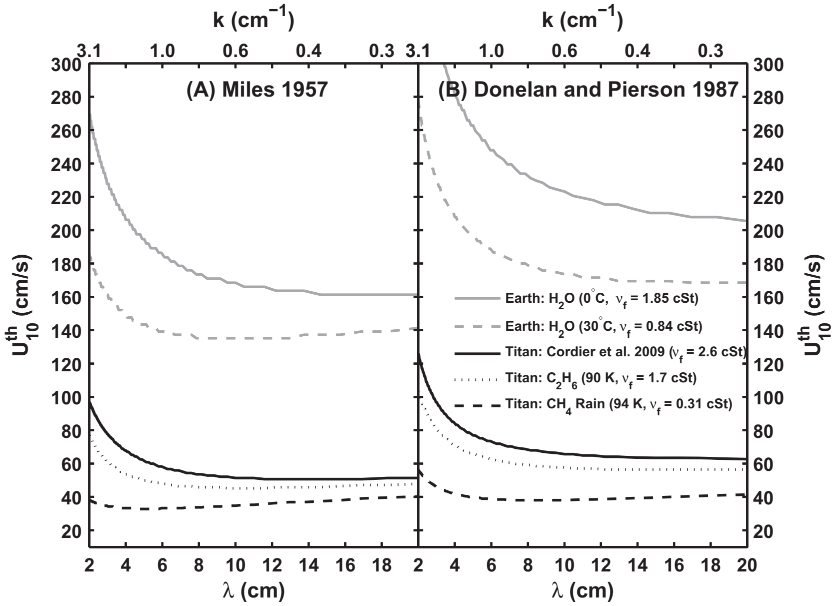

Fig. 3. Threshold wind speed at 10 m $\left(U_{10}^{th}\right)$ where the exponential growth rate of capillary-gravity waves is balanced by viscous dissipation. (A) U_{10}^{th} calculated from the theoretical model of Miles (1957). (B) $U_{10_{th}}$ calculated from the semi-empirical theory of Donelan and Pierson (1987)

$$n = 3.85\left|2 - \frac{1+3(k/k_{\min})^2}{1+(k/k_{\min})^2}\right|^3 + 1.15, \tag{3.2}$$

$$\ln\alpha = 17.4\left|2 - \frac{1+3(k/k_{\min})^2}{1+(k/k_{\min})^2}\right|^3 + 4.6. \tag{3.3}$$

While it is unknown how the specifics of wave breaking and non-linear wave–wave interactions of liquid hydrocarbon on Titan differ from sea water on Earth, the geometrical nature of these processes suggests that n and α are independent of variations in liquid properties and depend primarily of the shape of the wave spectrum ($k/k_{\min}$). The experiments required to validate this and other assumptions discussed herein, while important, are outside the scope of this work.

At any given wavenumber, non-zero spectral amplitude requires both $U_{\lambda/2} > c$ and a growth rate (Eq. (2.6)) that exceeds loss from viscous dissipation (Eq. (2.5)). Since, for the same wind velocity, phase speeds are ~2 times slower on Titan than Earth and the air-to-liquid density ratio is ~6.5 times higher (using the parameters listed in Table 1), we can expect capillary-gravity waves to grow both faster and larger in Titan's hydrocarbon seas (Eq. (2.6)).

For the longer wavelength end of the spectrum, we adopt the semi-empirically derived equilibrium spectrum of Donelan et al. (1985) for a fully developed wind-generated sea:

$$\Phi(k,\chi)_{long} = k^{-4}\left\{1.35\times10^{-3}\sqrt{k/k_p}e^{-(k_p/k)^2}1.7^{F(k/k_p)}h(k/k_p)\mathrm{sech}^2[h(k/k_p)(\chi-\bar{\chi})]\right\} \tag{3.4}$$

where

$$F(k/k_p) = e^{-1.22\left(\sqrt{k/k_p}-1\right)^2} \tag{3.5}$$

and $h(k/k_p)$ is defined as

$$h(k/k_p) = \begin{cases} 1.24, & \text{if } 0 < k/k_p < 0.31, \\ 2.61(k/k_p)^{0.65}, & \text{if } 0.31 < k/k_p < 0.90, \\ 2.28(k/k_p)^{-0.65}, & \text{if } 0.90 < k/k_p < 10. \end{cases} \tag{3.6}$$

The peak of the spectrum is given by:

$$k_p = g/(1.2U_{10})^2. \tag{3.7}$$

At low wavenumbers, both viscous dissipation and direct forcing from the wind are unimportant (Donelan and Pierson, 1987). The complete wave spectrum is a combination of Eqs. (3.4) and (3.1), with Eq. (3.4) valid for $k < 10k_p$ and Eq. (3.1) valid for $k \geqslant 10k_p$. The dimensionless constants listed in Eqs. (3.1)–(3.7) are assumed to be independent of changes in liquid and/or atmospheric properties (Donelan and Pierson, 1987).

The strength of a wave field can be characterized by its significant wave height ($H_{1/3}$). The significant wave height is defined as the average amplitude (peak-to-trough) of the highest third of the waves in a given wave field (Munk, 1944). In modern oceanography, however, $H_{1/3}$ is usually defined as four times the standard deviation of the surface elevation (e.g., Kinsman, 1984). In addition to $H_{1/3}$, a wave field's strength is also gauged by its slope distribution, which is typically expressed by the upwind and cross-wind mean squared topographic slopes (σ_u^2 and σ_c^2). The slope distribution is essential to understanding the radar backscatter and glint characteristics of a wave field.

The significant wave height ($H_{1/3}$) and mean squared slopes (σ_u^2, σ_c^2) can be approximated by direct integration of the complete wave spectrum (Eqs. (3.1) and (3.4)) following Valenzuela (1978):

$$H_{1/3}^2 = 16\int_{-\pi}^{\pi}\int_0^{\infty}\Phi(k,\chi)k\,dk\,d\chi, \tag{3.8}$$

$$\sigma_u^2 = \int_{-\pi}^{\pi}\int_0^{k_o/\Gamma}\Phi(k,\chi)k^2\cos^2\chi k\,dk\,d\chi, \tag{3.9}$$

$$\sigma_c^2 = \int_{-\pi}^{\pi}\int_0^{k_o/\Gamma}\Phi(k,\chi)k^2\sin^2\chi k\,dk\,d\chi, \tag{3.10}$$

where σ_u is the upwind RMS slope, σ_c is the crosswind RMS slope, k_o is the wavenumber of observation, and Γ is a constant used as a low pass filter (Donelan and Pierson, 1987). The result of integrating over the wave spectrum (Eqs. (3.1) and (3.4)) in Eq. (3.8) suggests that the significant wave height scales inversely with gravity and, for the same wind speed, is ~7 times greater on Titan than on Earth. Similarly, σ_u and σ_c calculated from Eqs. (3.9) and (3.10) are greater by a factor of ~2 on Titan for $U_{10} < 5$ m/ s. While the air–liquid density ratio affects the growth rate of capillary-gravity waves, it does not significantly affect their limiting steepness—this follows the strictly geometrical Stokes limit (see, e.g., Kinsman, 1984). Consequently, for a given wind speed, there will be many more breaking waves (white-caps) on Titan than on Earth.

4. Observing waves

Over Earth's oceans, Walsh et al. (1998) observed RMS slopes of $\sim 4°$ at Ka band (0.8 cm wavelength) under light winds near the onset of exponential capillary-gravity wave growth ($U_{10} \sim 1.6$ m/s). This is consistent with Eq. (3.9) using the wave spectrum defined in the previous section and $\Gamma = 40$. Given that Eqs. (3.9) and (3.10) predict slopes to be steeper on Titan and that near infrared wavelengths interact with more of the wave spectrum (larger k_o), the RMS slope of 0.15° derived by Barnes et al. (2011) for Kraken Mare and Jingpo Lacus on Titan is consistent with a complete lack of wind wave activity and suggests wind-speeds below the threshold for exponential growth (Fig. 3). In the presence of waves, glint measurements taken by the Visual and Infrared Mapping Spectrometer (VIMS) should indicate RMS slopes of at least a few degrees. Lower values, however, may be expected if waves are only present in a small portion of the footprint, which would suggest spatial variability in the wind and wind speeds near the onset of capillary-gravity wave growth. Shankaranarayanan and Donelan (2001) find that wind-speeds on Earth have significantly more variability, both spatially and temporally, near the threshold for wind wave generation.

Andreas and Wang (2007) note that, in terrestrial seas, $H_{1/3}$ is typically independent of wind-speed for $U_{10} < 4$ m/s. This is attributed to the presence of swells created during previous episodes of enhanced wind activity that have yet to dissipate. On Titan, a similar phenomenon may increase the observed significant wave heights during light winds (even for winds below the wave-generation threshold) during seasons of enhanced activity. For light winds in shallow areas, Andreas and Wang (2007) find that $H_{1/3}$ is primarily controlled by water depth, where interaction with the sea-floor can dissipate larger amplitude waves. As discussed in below, however, the Ku-band radar response of the wave-field is primarily controlled by smaller capillary-gravity waves near the Bragg frequency which, in the absence of forcing, will quickly lose energy through viscous dissipation.

While specular observations, such as altimetry (e.g. Wye et al., 2009) or glint (e.g., Barnes et al., 2011) measurements will be sensitive to even the smallest capillary-gravity waves excited by exponential feedback mechanisms, it is unclear whether or not wave fields on Titan will be observable to the Cassini RADAR at off-nadir geometries. At moderate incidence angles (10–60°) microwave backscatter is dominated by Bragg scatter. In a broad spectrum wave field, however, the smaller Bragg-scattering waves are tilted by their larger counterparts. In order to accurately estimate the radar backscatter of such a complex wavy surface, a composite model is required in which the effect of low frequency waves is taken into account. In such a model, the high wavenumber portion of the spectrum is used to estimate the power spectral amplitude at the Bragg wavenumber ($k_b = 2k\sin(\theta)$), while the low wavenumber portion of the spectrum is used to generate a slope distribution that describes the orientation of surface facets.

In order to estimate the Ku-band response of waves on Titan lakes, we adopt the composite backscatter model described in Donelan and Pierson (1987). Eq. (3.1) is used to estimate the spectral amplitude at the Bragg frequency, while Eq. (3.4) is used to determine the distribution of surface facets tilting the shorter waves. Surface facets are oriented using a Gaussian probability distribution defined by the mean square slope (σ_u, σ_c) and significant wave height ($H_{1/3}$). In addition to the longer-wavelength tilting of the Bragg scattering waves, the model also includes a specular component approximated by a Gaussian quasi-specular model (Hargreaves, 1959) and an estimate of wind gustiness following the measurements of Smith (1974). The framework and governing equations of the model are described in Donelan and Pierson (1987).

The results of the composite backscatter model are presented in Fig. 4. Between 10° and 60° incidence, the decrease in dielectric constant (ϵ) between water and liquid hydrocarbon results in an 8–15 dB decrease in the Fresnel reflectivity at horizontal polarization. For Bragg scatter on Titan, this decrease is partially offset by the increase in spectral power at the Bragg frequency resulting from the increased atmosphere-to-liquid density ratio and reduced wave phase speed relative to Earth (see Eq. (2.6)). Nevertheless, the backscatter cross-sections (σ_o) expected from hydrocarbon wave fields on Titan are low. For wind speeds below ~ 1 m/s and incidence angles greater than 20°, predicted σ_o values are less than-25 dB, which is below the noise floor of most Cassini SAR image pixels (Fig. 4). In scatterometry mode, however, the Cassini RADAR can measure σ_o values as low as -40 to -50 dB (West et al., 2008) which, according to the two-scale backscatter model, is sensitive enough to detect the presence or absence of waves within the ~ 10 km real-apertures footprint.

5. Predicted wind speeds

Lorenz et al. (2010b, 2012) discuss predicted wind speeds for Titan's polar regions based on the Köln and TitanWRF General Circulation Models (GCMs) described in Tokano (2009) and Newman et al. (2008), respectively. In each case, they report wind speeds in the lowest available altitude bin (300 m for Köln, 90 m for TitanWRF). As a heuristic, one may use an empirical law for Earth applications to estimate the wind speed variation with height below the lowest model level, i.e., $U(z) \approx U_{10}(z/z_{10})^p$, where z_{10} is the reference height (10 m) and $p \sim 0.11$ (e.g., Hsu et al., 1994). This correction suggests factors of ~ 0.69 and ~ 0.79 should be applied, respectively, to the Köln and TitanWRF results cited in Lorenz et al. (2010b, 2012) to obtain estimates for U_{10}.

Both models predict polar winds that are calm during the winter months (wind speeds generally below 0.4 m/s) but increase during the spring/summer to as high as 1.2 m/s (corrected to 10 m) near solstice (Lorenz et al., 2010b). In general, the TitanWRF GCM predicts calmer winds than the Köln model. A more recent GCM described by Schneider et al. (2012) produces calmer winds than both models. Future observations discerning the presence or absence of waves during the upcoming Titan summer may help to distinguish amongst available GCMs by comparing predicted wind speed distributions to observed wave temporal frequency and amplitude.

As discussed in Lorenz et al. (2012), the wind speeds for Ligeia Mare in late summer ($L_s = 160°$, where L_s is the planetocentric solar longitude) are rather similar in the Köln and TitanWRF models. An inspection of the time histories, however, shows a substantially later onset of strong summer winds in the Köln model. Since Cassini observations cannot be uniquely interpreted in terms of quantitative surface wind speeds without knowing the liquid viscosity, the timing of the seasonal increase in wind speed may be the most useful discriminator of the predictive success of these GCMs.

Herein we use the three dimensional Titan GCM of Schneider et al. (2012), set to report Earth-daily (24 h) averaged wind speeds at an elevation of 10 m above the surface (see Fig. 5), allowing direct comparison to Fig. 3. The U_{10} winds are obtained from the friction velocity ($u_\star$) produced by the model and a logarithmic velocity profile (Eq. (2.3)) with a fixed roughness length of $z_o = 0.5$ -cm as is assumed by the GCM. Because the friction velocity (i.e., surface stress at a given location) balances the angular momentum flux convergence in the atmospheric columns aloft, and because this angular momentum flux convergence is affected by large-scale dynamics, the friction velocity is likely a more robust model result

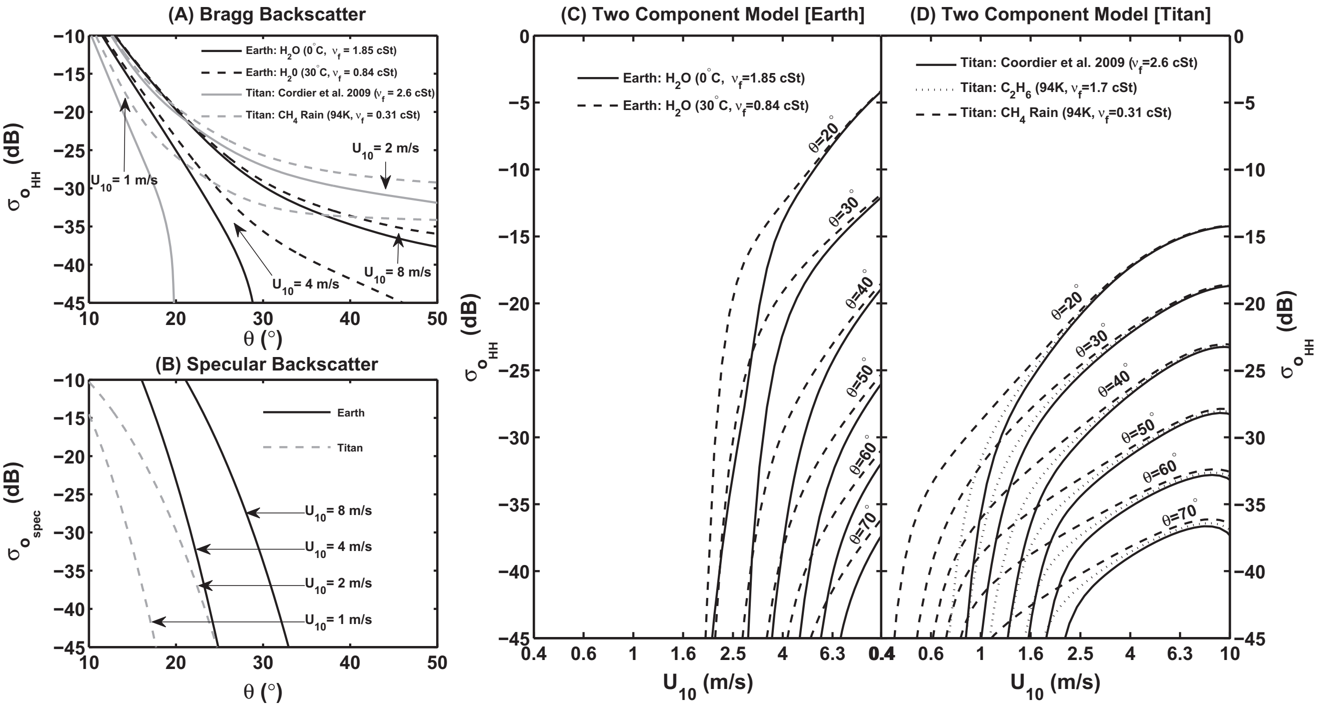

Fig. 4. Two-component Ku-band backscatter model of Donelan and Pierson (1987) adapted to Titan conditions for upwind azimuth geometry. Normalized backscatter cross-sections (σ_o) are shown for horizontal polarization, corresponding to the primary orientation of the Cassini RADAR while in Synthetic Aperture Radar (SAR) mode. Results for vertical polarization are similar. (A) Bragg backscatter component. (B) Specular backscatter component. (C/D) Two-component model taking into account both Bragg and specular terms, the tilting effects of longer period gravity waves, and an estimation of the wind vector's gustiness. Panel C uses Earth-relevant parameters while panel D depicts response in the Titan environment.

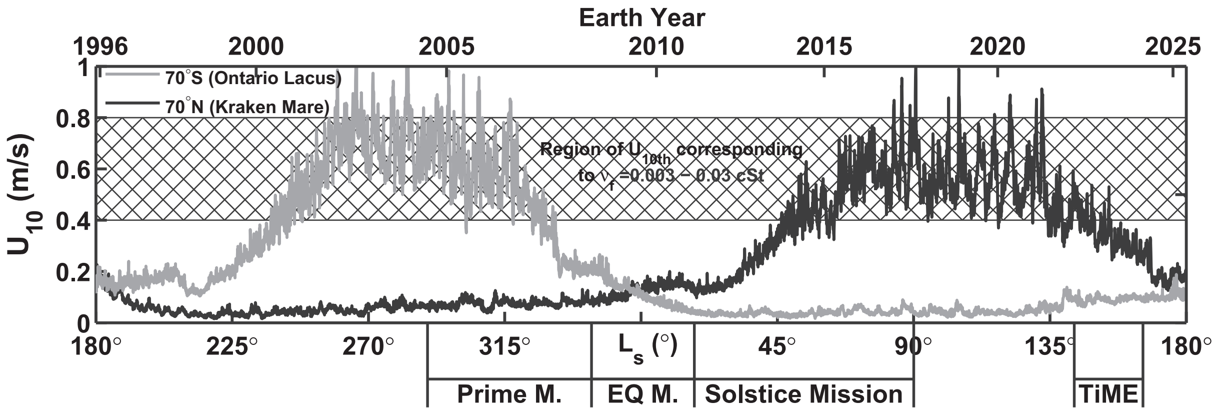

Fig. 5. Wind speeds averaged over 24 h at 10 m from Schneider et al. (2012) using a three-dimensional Titan GCM. Values represent the 95% quantile of the longitudinal distribution at 70°S and 70°N for a given time after averaging over five seasonal cycles. The cross-hatched region highlights the expected range of threshold wind speeds for ν_f = 0.003–0.03 cm^2/s. Wind speeds are expected to exceed threshold during the spring/summer but remain below even the minimum threshold during each pole's respective equinox and winter. The L_s ranges of the Cassini Prime, Equinox, and Solstice Missions, as well as the arrival window of the proposed TiME mission, are shown at the bottom of the figure.

that is less dependent, e.g., on how boundary layer turbulence is represented than are low-level winds. It should be noted, however, that, to the extent that poorly constrained boundary layer dynamics can affect the angular momentum flux aloft (e.g., mesoscale sea breeze circulations), model results may differ from the local environment. Including the effects of local-scale features, such as isolated lakes or mountains, in GCM calculations will enhance their ability to accurately predict wind speeds over Titan's hydrocarbon liquids. On Earth, temperature differences of ~10 K between the land and ocean result in pressure differences that generate land and sea breezes with magnitudes of up to ~10 m/s (Simpson, 1994). While physical temperature differences on Titan are expected to be low (at most 1–3 K) (Jennings et al., 2009) and predicted sea breeze magnitudes small (<1 m/s) (Tokano, 2009), land and/or sea breezes may increase winds in the vicinity of shorelines.

Compared with the Köln and TitanWRF GCMs, Schneider et al. (2012) predict slightly lower wind speeds, although these differences are somewhat reduced by referencing reported wind speeds to a common elevation of 10 m using the boundary layer correction discussed above. Remaining variations may be due to the differences between the statistical metrics used to generate reported values as well as fundamental differences amongst the models. In this work, outputs from the Schneider et al. (2012) GCM are averaged over five Titan years. In an attempt to simplify the high quantity of data produced by the GCM, we compared our estimates of wind threshold $\left(U_{10}^{th}\right)$ against the 95% quantile of the longitudinal distribution of daily-average surface winds at 10 m for a given latitude and time. These winds should be representative of the gustier conditions observed by Cassini if GCM predictions are accurate. One should bear in mind, however, that there are calm days during windy seasons (and vice versa) and some care should be taken in drawing too strong conclusions about Titan's winds (or models thereof) from a small number of point observations by Cassini. To formally assess the winds from detections or non-detections of waves, a probabilistic (e.g., Bayesian) approach will need to be adopted once sufficient data are available.

Poleward of 50°, the GCM reports wind-speeds below the predicted thresholds for wave generation between autumnal and vernal equinox in each hemisphere. All of the Cassini measurements reported to observe an absence of wave activity were acquired during this time period. However, for spring/summer ($\sim 60^\circ < L_s \lesssim 150^\circ$ in the north or $\sim 240 < L_s \lesssim 330^\circ$ in the south), wind speeds exceeding the minimum threshold of 0.4 m/s (pure methane) are predicted in the polar regions. The predicted wind speeds for 70°S (Ontario Lacus) and 70°N (Kraken Mare) are depicted in Fig. 5. The cross-hatched region of Fig. 5 represents the range of threshold wind speeds derived using Eq. (2.6). During spring and summer in each hemisphere, wind speeds span the range of the predicted thresholds. At 80°N, which is the latitude of Ligeia Mare, predicted wind speeds in spring/summer are ~27% lower than at 70°N. Ligeia Mare is the primary target for the Titan Mare Explorer (TiME), a proposed Discovery-class mission to land a capsule in a Titan lake in 2023 (Stofan et al., 2011). In 2023 the predicted U_{10} at 80°N from Schneider et al. (2012) is $0.33^{+0.14}_{-0.10}$ m/s, near the minimum threshold for capillary-gravity wave growth. Lorenz et al. (2012) report wind speeds as high as 1 m/s at 300 m (occurring 5% of the time) using the Köln GCM of Tokano (2009), corresponding to $U_{10} \sim 0.7$ m/s. The significant wave heights to which gravity waves might grow in these or higher winds, and the probability distribution of individual ('rogue') wave heights given a significant wave height are discussed in a separate paper (Lorenz and Hayes, 2012).

6. Discussion

The first direct attempt to detect wave activity on Titan was performed by Wye et al. (2009), who showed that Ontario Lacus had a maximum root-mean-square (RMS) roughness of 3 mm over the ~100 m Fresnel zone during the December 2008 (T49) altimetry pass. In July 2009, the VIMS instrument observed glints from the northern seas Kraken Mare and Jingpo Lacus (Stephan et al., 2010). Barnes et al. (2011) analyzed the glints and found that the RMS surface slope was at most 0.15° over the ~1 km specular footprints during image acquisition. Both of these observations suggest a complete absence of wave activity, consistent with the calm surface winds predicted by available GCMs near equinox (Fig. 5). Upcoming observations during northern spring and summer, however, are predicted to exceed the expected threshold speeds of 0.4–0.7 m/s for compositions ranging from pure methane rain (25% nitrogen and 75% methane) to atmospheric equilibrium (Cordier et al., 2009), varying with liquid viscosity. Thus, the presence or absence of wave activity during the Cassini Solstice Mission may provide information constraining both the wind regime and composition of Titan's polar lakes and seas. The absence of surface waves could be the result of calm winds, highly viscous fluids, or surfactants inhibiting the growth of capillary-gravity waves. The presence of waves, on the other hand, will suggest winds exceeding the predicted threshold and a lack of appreciable surfactants. If an independent estimate of wind speed can be provided, the presence of wind waves will suggest a maximum viscosity for the lake. Similarly, the absence of waves can provide an estimate for the minimum possible liquid viscosity.

It should be noted, however, that the viscosities pertaining to the Cordier et al. (2009) compositions are not a strict upper limit. As discussed in Lorenz et al. (2010b), Cordier et al. (2009) assume thermodynamic equilibrium with the atmosphere for the main constituents while the abundance of minor components (notably propane and butane, which have the largest effect on viscosity) are estimated from the flux in a photochemical model. Any difference in the assumed photochemical flux could lead to differences in the concentration of the heavier compounds that increase viscosity. Similarly, if there are large-scale migrations of liquid from one pole to another on astronomical timescales (10^4–10^5 yrs), as suggested by Aharonson et al. (2009), we may expect a fractionation of liquid composition as lakes in the drying pole become enriched in heavier, more viscous compounds. Thus the wind threshold for waves may be different between the northern and southern hemispheres. Given morphological indications that the north is gaining liquid at the expense of the south (e.g., drowned river valleys in the margins of the northern seas (e.g., Cartwright et al., 2011), and a playa-like morphology (Lorenz et al., 2010a), evidence for paleoshorelines (Barnes et al., 2009) and shallow depth (Hayes et al., 2010) at Ontario Lacus), we would accordingly predict the present-day threshold to be higher in the south than in the north. This of course does not exclude a lower threshold in the past (in fact, it implies it), which could help to explain the shorelines morphologies interpreted as wave-cut beaches at Ontario Lacus by Wall et al. (2010). For liquid compositions more viscous than those predicted by Cordier et al. (2009) ($\nu_l > 0.026$ cm^2/s), the Donelan and Pierson (1987) model predicts a power law relationship between viscosity and threshold wind speed given by $U_{10}^{th}(\nu_f) \approx 264 \times \nu_f^{0.57\pm0.03} + U_{10}^{th}(\nu_{CH_4})$. For extreme viscosities of 10–100 times that of seawater at 30°C, the predicted U_{10}^{th} for liquid hydrocarbon compositions range from 1 to 3 m/s. At even larger viscosities, U_{10}^{th} increases to the point were the Kelvin–Helmholtz mechanism, which is independent of ν_l and requires $U_{10} > 3$ m/s, becomes the likelier wave generation mechanism. As discussed in Section 5, however, the highest wind speeds expected on Titan are $U_{10} \sim 1$ m/s.

While altimetry observations are sensitive to wave heights comparable to the radar's 2 cm wavelength, SAR observations are hindered by the low Fresnel reflectivity of liquid hydrocarbon. When applied to Titan, the two-scale model of Donelan and Pierson (1987) predicts off-axis backscatter ($\theta > 20^\circ$) below −20 dB for $U_{10} < 2$ m/s. Thus, wave activity may be below the noise equivalent backscatter ($\sigma_{o_{NE}}$) of SAR images, which can range between −15 and −25 dB depending on observational geometry. On the other hand, while the radiometric sensitivity of SAR images (at the pixel scale) may be marginal for detecting waves, larger-scale morphological indications may help—darker regions in the lee of islands or mountains may indicate topographic sheltering and thus not only the presence of waves, but also the wind direction. We suggest, based on the results of a two-scale backscatter model, that SAR observations of the seas be made at as low an incidence angle as possible. Additionally, for the larger lakes and seas, where the radar's ~10 km real-aperture beam footprint can be fully contained within a sea's perimeter, the real-aperture noise floor is closer to −40 or −50 dB, and thus scatterometry measurements (which are routinely used to estimate sea-surface winds from wave steepness on Earth) may better quantify waves. VIMS glint observations, which have surface footprints of order 1 km, are able to measure RMS surface slopes to a precision of 0.1° or better (Barnes et al., 2011). As wind waves on Titan are predicted to produce RMS slopes of at least a few degrees, they should be observable to VIMS when it observes at specular geometries. While the Imaging Science Subsystem has the sensitivity to observe specular reflection from Titan's surface (e.g., West et al., 2005), atmospheric scattering at 938 nm limits surface observations to emission angles below ~40°, which is less than the minimum solar incidence over Titan's polar lake districts (Turtle, E.P., personal email communication, 2012).

7. Summary

In summary, while the low reflectivity of liquid hydrocarbon will make it difficult to observe the spatial structure of wind wave behavior in SAR images, the presence or absence of wind waves during Cassini's Solstice Mission should be discernable on a number of occasions from altimetry, scatterometry, binned-SAR, and/or observations of infrared glints. Furthermore, the presence or absence of waves may provide constraints on the composition of Titan's hydrocarbon seas and/or help to discriminate amongst available GCMs. Polar winds during upcoming Northern Spring/Summer are predicted to exceed modeled wave generation thresholds of $U_{10}^{th} = 0.4 - 0.7$ m/s for liquids ranging from methane rain to the more complex compositions described in Cordier et al. (2009). The wave generation threshold for ethane, which is generally considered the primary constituent of the large seas (e.g., Hayes et al., 2011), is $U_{10}^{th} = 0.6$ m/s. Finally, Cassini may only represent the beginning of Titan wave studies. Future missions concepts include orbiters better suited to repeat observation of the sea surface (e.g., Lorenz et al., 2008; Sotin et al., 2011), airplanes (e.g., Barnes et al., 2010), or floating capsules (e.g., Stofan et al., 2011) that can observe wave fields in situ.

Acknowledgments

A.G.H. would like to the thank the Miller Institute for Basic Research in Science for partially funding this work. R.L., J.I.L., and P.E. were partially supported by the Cassini Project (for R.L. via NASA Grant NNX13AH 14G). T.S. and S.D.G. acknowledge support from a NASA Earth and Space Science Fellowship and a David and Lucile Packard Fellowship. We would especially like to thank and acknowledge H.E. Schlichting of the Massachusetts Institute of Technology for her advice and contributions to this work and Richard Lovelace of Cornell University, whose inquiries supplied the motivation for this project. All authors would also like to thank the Cassini engineering team, without whom this manuscript would not have been possible.

References

Aharonson, O., Hayes, A.G., Lunine, J.I., Lorenz, R.D., Allison, M.D., Elachi, C., 2009. An asymmetric distribution of lakes on Titan as a possible consequence of orbital forcing. Nat. Geosci. 2, 851–854. http://dx.doi.org/10.1038/ngeo698.

Andreas, Edgar L., Wang, Sinny, 2007. Predicting significant wave height off the northeast coast of the United States. Ocean Eng. 34, 1328–1335. http://dx.doi.org/10.1016/j.oceaneng.2006.08.004, ISSN 0029-8018. <http://www.sciencedirect.com/science/article/pii/S0029801806002332>.

Banfield, D., Donelan, M.A., Cavaleri, L., 2012. Winds, waves and shorelines from ancient martian seas. AAS/Division for Planetary Sciences Meeting, vol. 44. Bulletin of the American Astronomical Society, p. 1019 (abstracts).

Barenblatt, G.I., Chorin, A.J., 1998. New perspectives in turbulence: Scaling laws, asymptotics, and intermittency. SIAM Rev. 40, 265–291. http://dx.doi.org/10.1137/S0036144597320047.

Barnes, J.W., Brown, R.H., Soderblom, J.M., Soderblom, L.A., Jaumann, R., Jackson, B., Le Mouélic, S., Sotin, C., Buratti, B.J., Pitman, K.M., Baines, K.H., Clark, R.N., Nicholson, P.D., Turtle, E.P., Perry, J., 2009. Shoreline features of Titan's Ontario Lacus from Cassini/VIMS observations. Icarus 201, 217–225. http://dx.doi.org/10.1016/j.icarus.2008.12.028.

Barnes, J.W., McKay, C., Lemke, L., Beyer, R.A., Radebaugh, J., Atkinson, D., 2010. AVIATR: Aerial vehicle for in-situ and airborne titan reconnaissance. Lunar Planet. Sci. 41, 2551 (abstract).

Barnes, J.W., Soderblom, J.M., Brown, R.H., Soderblom, L.A., Stephan, K., Jaumann, R., Mouélic, S.L., Rodriguez, S., Sotin, C., Buratti, B.J., Baines, K.H., Clark, R.N., Nicholson, P.D., 2011. Wave constraints for Titan's Jingpo Lacus and Kraken Mare from VIMS specular reflection lightcurves. Icarus 211, 722–731. http://dx.doi.org/10.1016/j.icarus.2010.09.022.

Brown, R.H. et al., 2008. The identification of liquid ethane in Titan's Ontario Lacus. Nature 454, 607–610.

Businger, J.A., 1973. Turbulent transfer in the atmospheric surface layer. In: Haugen, D.A. (Ed.), Workshop on Micrometeorology. American Meteorological Society, pp. 67–100.

Cartwright, R., Clayton, J.A., Kirk, R.L., 2011. Channel morphometry, sediment transport, and implications for tectonic activity and surficial ages of Titan basins. Icarus 214, 561–570. http://dx.doi.org/10.1016/j.icarus.2011.03.011.

Charnock, H.A., 1955. Wind stress on a water surface. Q. J. R. Meteorol. Soc. 81, 639–640. http://dx.doi.org/10.1002/qj.49708135027.

Cordier, D., Mousis, O., Lunine, J.I., Lavvas, P., Vuitton, V., 2009. An estimate of the chemical composition of Titan's lakes. Astrophys. J. 707, L128–L131. http://dx.doi.org/10.1088/0004-637X/707/2/L128.

Donelan, M.A., Pierson, W.J., 1987. Radar scattering and equilibrium ranges in wind-generated waves with application to scatterometry. J. Geophys. Res. 92, 4971–5030. http://dx.doi.org/10.1029/JC092iC05p04971.

Donelan, M.A., Plant, W.J., 2009. A threshold for wind-wave growth. J. Geophys. Res. 114 (C13), C07012. http://dx.doi.org/10.1029/2008JC005238.

Donelan, M.A., Hamilton, J., Hui, W.H., 1985. Directional spectra of wind-generated waves. R. Soc. Lond. Philos. Trans. Ser. A 315, 509–562. http://dx.doi.org/10.1098/rsta.1985.0054.

Elliot, J.A., 1972. Microscale pressure fluctuations measured within the lower atmosphere boundary layer. J. Fluid Mech. 53, 351–383.

Garratt, J.R., 1977. Review of drag coefficients over oceans and continents. Mon. Weather Rev. 105, 915, http://dx.doi.org/10.1175/1520-0493(1977)105<0915:RODCOO>2.0.CO;2.

Ghafoor, N.A.-L., Zarnecki, J.C., Challenor, P., Srokosz, M.A., 2000. Wind-driven surface waves on Titan. J. Geophys. Res. 105, 12077–12092. http://dx.doi.org/10.1029/1999JE001066.

Hargreaves, J.K., 1959. Radio observations of the lunar surface. Proc. Phys. Soc. Lond. B73, 536–537.

Hayes, A.G. et al., 2010. Bathymetry and absorptivity of Titan's Ontario Lacus. J. Geophys. Res.: Planets 115, E09009. http://dx.doi.org/10.1029/2009JE003557.

Hayes, A.G., Aharonson, O., Lunine, J.I., Kirk, R.L., Zebker, H.A., Wye, L.C., Lorenz, R.D., Turtle, E.P., Paillou, P., Mitri, G., Wall, S.D., Stofan, E.R., Mitchell, K.L., Elachi, C.The Cassini RADAR Team, 2011. Transient surface liquid in Titan's polar regions from Cassini. Icarus 211. http://dx.doi.org/10.1016/j.icarus.2010.07.017.

Hsu, S.A., Meindl, E.A., Gilhousen, D.B., 1994. Determining the power-law wind-profile exponent under near-neutral stability conditions at sea. J. Appl. Meteorol. 33, 757–772, http://dx.doi.org/10.1175/1520-0450(1994)033<0757:DTPLWP>2.0.CO;2.

Jeffreys, H., 1924. On the formation of waves by wind. Proc. R. Soc. Lond. Ser. A 107, 189–206.

Jennings, D.E. et al., 2009. Titan's surface brightness temperatures. Astrophys. J. 691, L103–L105. http://dx.doi.org/10.1088/0004-637X/691/2/L103.

Kahma, K.K., Donelan, M.A., 1988. A laboratory study of the minimum wind speed for wind wave generation. J. Fluid Mech. 192, 339–364. http://dx.doi.org/10.1017/S0022112088001892.

Kinsman, B., 1984. Wind Waves: Their Generation and Propogation on the Ocean surface. Prentace-Hall, ISBN 0486646521.

Lighthill, M.J., 1962. Physical interpretation of the mathematical theory of wave generation by wind. J. Fluid Mech. 14, 385–398. http://dx.doi.org/10.1017/S0022112062001305.

Lorenz, R.D., Hayes, A.G., 2012. The growth of wind-waves in Titan's hydrocarbon seas. Icarus 219, 468–475. http://dx.doi.org/10.1016/j.icarus.2012.03.002.

Lorenz, R.D., Kraal, E.R., Eddlemon, E.E., Cheney, J., Greeley, R., 2005. Sea-surface wave growth under extraterrestrial atmospheres: Preliminary wind tunnel experiments with application to Mars and Titan. Icarus 175, 556–560. http://dx.doi.org/10.1016/j.icarus.2004.11.019.

Lorenz, R.D. et al., 2006. The sand seas of Titan: Cassini RADAR observations of longitudinal dunes. Science 312, 724–727. http://dx.doi.org/10.1126/science.1123257.

Lorenz, R.D., Leary, J.C., Lockwood, M.K., Waite, J.H., 2008. Titan Explorer: A NASA Flagship Mission Concept. In: El-Genk, M.S. (Ed.), Space Technology and Applications International Forum-STAIF 2008. American Institute of Physics Conference Series, vol. 969, pp. 380–387. http://dx.doi.org/10.1063/1.2844991.

Lorenz, R.D., Jackson, B., Hayes, A., 2010a. Racetrack and Bonnie Claire: Southwestern US playa lakes as analogs for Ontario Lacus, Titan. Planet. Space Sci. 58, 724–731. http://dx.doi.org/10.1016/j.pss.2009.05.012.

Lorenz, R.D., Newman, C., Lunine, J.I., 2010b. Threshold of wave generation on Titan's lakes and seas: Effect of viscosity and implications for Cassini observations. Icarus 207, 932–937. http://dx.doi.org/10.1016/j.icarus.2009. 12.004.

Lorenz, Ralph D., Tokano, Tetsuya, Newman, Claire E., 2012. Winds and tides of Ligeia Mare, with application to the drift of the proposed time TiME (Titan Mare Explorer) capsule. Planet. Space Sci. 60 (1), 72–85. http://dx.doi.org/10.1016/j.pss.2010.12.009.

Miles, J.W., 1957. On the generation of surface waves by shear flows. J. Fluid Mech. 3, 185–204. http://dx.doi.org/10.1017/S0022112057000567.

Miles, J.W., 1959. On the generation of surface waves by shear flows. Part 3. Kelvin–Helmholtz instability. J. Fluid Mech. 6, 583–598. http://dx.doi.org/10.1017/S0022112059000842.

Munk. W.H., 1944. Proposed uniform procedure for observing waves and interpreting instrument records. In: Scripps Institute of Oceanography Wave Reports, vol. 44-25. Declassified US Document, 28pp.

National Renewable Energy Laboratory, 1997. Wind resource assessment handbook. Technical Report NREL-TAT-5-12283-01, National Renewable Energy Laboratory, 1617 Cole Boulevard, Golden, CA 80401.

Newman, C.E., Richardson, M.I., Lee, C., Toigo, A.D., Ewald, S.P., 2008. The TitanWRF Model at the end of the Cassini Prime Mission. AGU (Fall Meet.), p. A2 (abstracts).

Nikuradse, A., 1933. Zur Deutung des Funkenentladungsmechanismus. Z. Phys. 84, 701–704. http://dx.doi.org/10.1007/BF01330494.

Paillou, P. et al., 2008. Microwave dielectric constant of Titan-relevant materials. Geophys. Res. Lett. 35. http://dx.doi.org/10.1029/2008GL035216, L18202:1–L18202:4.

Phillips, O.M., 1957. On the generation of waves by turbulent wind. J. Fluid Mech. 2, 417–445. http://dx.doi.org/10.1017/S0022112057000233.

Plant, W.J., 1982. A relationship between wind stress and wave slope. J. Geophys. Res. 87, 1961–1967. http://dx.doi.org/10.1029/JC087iC03p01961.

Saxton, J.A., Lane, J.A., 1952. Electrical properties of seawater. Wireless Eng. 291, 269–275. http://dx.doi.org/10.1038/300731a0.

Schneider, T., Graves, S.D.B., Schaller, E.L., Brown, M.E., 2012. Polar methane accumulation and rainstorms on Titan from simulations of the methane cycle. Nature 481, 58–61. http://dx.doi.org/10.1038/nature10666.

Shankaranarayanan, K., Donelan, M.A., 2001. A probabilistic approach to scatterometer model function. J. Geophys. Res. 106, 19969–19990. http://dx.doi.org/10.1029/1999JC000189.

Shtemler, Y.M., Mond, M., Cherniavskii, V., Golbraikh, E., Nissim, Y., 2008. An asymptotic model for the Kelvin–Helmholtz and Miles mechanisms of water wave generation by wind. Phys. Fluids 20 (9), 094106. http://dx.doi.org/10.1063/1.2980350.

Simpson, J.E., 1994. Sea Breeze and the Local Wind. Cambridge University Press, ISBN 0-521-45211-2..

Smith, S.D., 1974. Eddy flux measurements over Lake Ontario. Bound.-Layer Meteorol. 6, 235–255. http://dx.doi.org/10.1007/BF00232487.

Smith, S.D., 1988. Coefficients for sea surface wind stress, heat flux, and wind profiles as a function of wind speed and temperature. J. Geophys. Res. 93, 15467–15472. http://dx.doi.org/10.1029/JC093iC12p15467.

Soderblom, J.M., Barnes, J.W., Soderblom, L.A., Brown, R.H., Griffith, C.A., Nicholson, P.D., Stephan, K., Jaumann, R., Sotin, C., Baines, K.H., Buratti, B.J., Clark, R.N., 2012. Modeling specular reflections from hydrocarbon lakes on Titan. Icarus 220, 744–751. http://dx.doi.org/10.1016/j.icarus.2012.05.030.

Sotin, C. et al., 2011. JET: Journey to Enceladus and Titan. Lunar Planet. Sci. 42, 1326 (abstracts).

Stephan, K. et al., 2010. Specular reflection on Titan: Liquids in Kraken Mare. Geophys. Res. Lett. 37, L07104. http://dx.doi.org/10.1029/2009GL042312.

Stofan, E.R. et al., 2011. The Titan Mare Explorer Mission (TiME): A discovery mission to a Titan sea. In: EPSC-DPS Joint Meeting 2011, 2–7 October 2011 in Nantes, France, p. 909. <http://meetings.copernicus.org/epsc-dps2011>.

Thomson, W, 1871. Hydrokinetic solutions and observations. Philos. Mag. 42, 362–377 (Lord Kelvin).

Tokano, T., 2009. Impact of seas/lakes on polar meteorology of Titan: Simulation by a coupled GCM-Sea model. Icarus 204, 619–636. http://dx.doi.org/10.1016/j.icarus.2009.07.032.

Valenzuela, G.R., 1978. Theories for the interaction of electromagnetic and oceanic waves – A review. Bound.-Layer Meteorol. 13, 61–85. http://dx.doi.org/10.1007/BF00913863.

Wall, S. et al., 2010. Active shoreline of Ontario Lacus, Titan: A morphological study of the lake and its surroundings. Geophys. Res. Lett. 37. http://dx.doi.org/10.1029/2009GL041821, L5202:1–L5202:5.

Walsh, E.J. et al., 1998. Observations of sea surface mean square slope under light wind during the Tropical Ocean-Global Atmosphere Coupled Ocean-Atmosphere Response Experiment. J. Geophys. Res. 1031, 12603–12612. http://dx.doi.org/10.1029/98JC00780.

Weast, R.C. (Ed.), 1984. CRC Handbook of Chemistry and Physics. A Ready-Reference Book of Chemical and Physical Data. Chemical Rubber Comp. Press.

West, R.A., Brown, M.E., Salinas, S.V., Bouchez, A.H., Roe, H.G., 2005. No oceans on Titan from the absence of a near-infrared specular reflection. Nature 436, 670–672. http://dx.doi.org/10.1038/nature03824.

West, R.D. et al., 2008. Cassini RADAR sequence planning and instrument performance. IEEE TGRS, pp. 1777–1795. http://dx.doi.org/10.1109/TGARS.2008.2007217.

Wye, L.C., Zebker, H.A., Lorenz, R.D., 2009. Smoothness of Titan's Ontario Lacus: Constraints from Cassini RADAR specular reflection data. Geophys. Res. Lett. 36. http://dx.doi.org/10.1029/2009GL039588, L16201:1–L16201:5.

Young, I.R., 1999. Wind generated ocean waves. Elsevier Ocean Engineering Book Series, vol. 2. Elsevier Science Ltd., ISBN 0-08-043317-0..